

Sea ice drift and its relationship to altimetry-derived ocean currents in the Labrador Sea

S. Häkkinen and D. J. Cavalieri

NASA Goddard Space Flight Center, Greenbelt, Maryland, USA

Received 10 February 2005; revised 4 May 2005; accepted 6 May 2005; published 11 June 2005.

[1] Low frequency sea ice drift variability and its oceanic and atmospheric forcing are investigated for the Labrador Sea over the period 1979–2002. Our objective is to separate the ocean forced component of ice drift in order to corroborate the changes in the subpolar gyre circulation found by Häkkinen and Rhines (2004). The atmospheric and oceanic forcing components can be approximately separated by comparing the time series resulting from an Empirical Orthogonal Function (EOF) analysis of sea ice motion with local sea level pressure gradients and altimetry-derived oceanic velocities. The first ice motion EOF is found to be associated with wind driven ice drift. The second mode is associated with oceanic forcing, because its time series is similar in its fluctuations to the oceanic velocities derived from altimetry. These two data sets confirm a major weakening of the subpolar ocean circulation between the early 1990s and the latter 1990s.

Citation: Häkkinen, S., and D. J. Cavalieri (2005), Sea ice drift and its relationship to altimetry-derived ocean currents in the Labrador Sea, *Geophys. Res. Lett.*, 32, L11609, doi:10.1029/2005GL022682.

1. Introduction

[2] High northern latitudes have witnessed a significant decrease in overall sea ice extent and ice thickness during our observational period 1979–2002 [e.g., Cavalieri *et al.*, 2003; Yu *et al.*, 2004]. There is, however, considerable variability within the Arctic sub-regions [Parkinson and Cavalieri, 2002]. In this study we focus on the Labrador Sea and its sea ice cover, which (jointly with the Baffin Bay ice cover) has shown a decrease over our study period, although the trend is not statistically significant [Parkinson and Cavalieri, 2002]. Besides the changes in the sea ice cover as deduced from satellite microwave radiometry, altimetry platforms like TOPEX/Poseidon and Jason-1 have provided a glimpse of the circulation changes at subpolar latitudes. The 1990s, in particular, showed a decline in the strength of the subpolar upper ocean circulation [Han and Tang, 2001; Häkkinen and Rhines, 2004]. The decline is difficult to explain by wind driven dynamics alone, so it has to involve large-scale oceanic circulation changes associated with stratification changes. As for the altimetry time series, unfortunately only fragmentary data from current meters are available to validate the altimetry-derived velocities. A goal of this study is to demonstrate the utility of sea ice drift data from the Labrador shelf to complement the open ocean currents derived from the discontinuous altimetry record.

[3] Here we analyze both the altimetry derived ocean currents (NASA Pathfinder Dataset) and sea ice motion data derived from satellite and in situ data sets [Fowler, 2003]. The only driving forces for sea ice drift are winds and ocean currents, thus there is a possibility to extract ocean current information from ice drift. We will show that in the Labrador Sea the ice drift can be divided approximately into atmosphere-driven and ocean-driven components. This task will be accomplished by applying EOF analysis to the sea ice motion and altimetry data sets. Links to atmospheric forcing are drawn by using geostrophic wind speed computed from sea level pressure fields. Ties to oceanic forcing are developed from comparisons with altimetric ocean currents and with iceberg drift.

2. Data Sets

[4] The sea ice motion data set used here was developed by Fowler [2003] and is available on a 25 km grid from the National Snow and Ice Data Center. The ice motion is derived from the NOAA Advanced Very High Resolution Radiometer (AVHRR), the Nimbus 7 Scanning Multichannel Microwave Radiometer (SMMR), the DMSP Special Sensor Microwave/Imager (SSM/I), and the International Arctic Buoy Programme (IABP) buoy data sets using cross-correlation techniques for the period November 1978 to March 2003. The maximum ice cover in the Labrador Sea is reached in late winter, so to maximize the number of grid points with drift data and to suppress high frequency variability, ice velocities were averaged from February to April retaining only grid points which had a non-zero ice velocity every year during those 3 months for the period 1979 to 2002. The mean February–April drift was removed before the EOF analysis. Another data set that provides potential insight into the changes in ocean circulation is the iceberg count crossing the 48°N latitude. This data set is maintained by the International Ice Patrol (<http://www.uscg.mil/lantarea/iip/home.html>).

[5] The ocean currents are computed based on the geostrophic balance from sea surface heights measured by altimeters. The altimetry data consist of the archived one-degree resolution TOPEX/Poseidon data, which have been combined with ERS-1/2 data to form the NASA Pathfinder data set. The Pathfinder data set also includes Seasat and Geosat data, which are referenced to TOPEX. The accuracy of the TOPEX/Poseidon altimeter is about 4 cm, whereas the Seasat and Geosat accuracies are of the order of 10 cm or more. Jason-1 data, which were processed similarly to the Pathfinder data set, were appended to the Pathfinder time

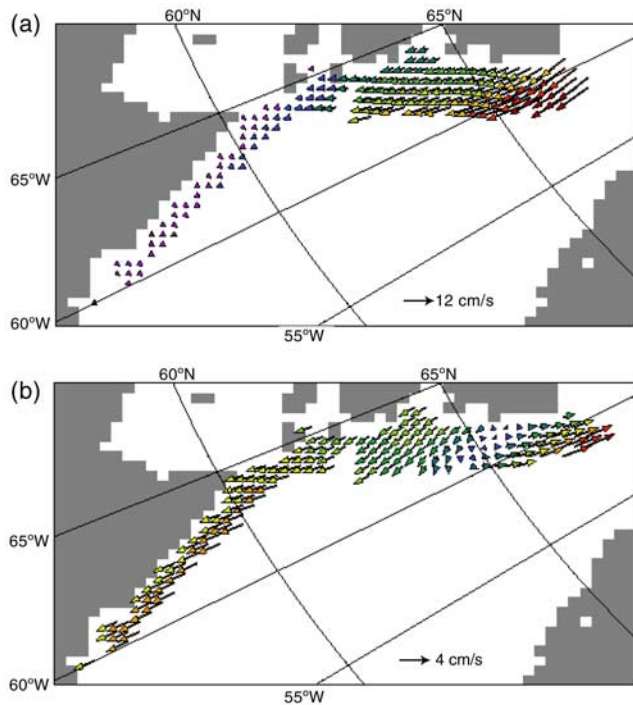


Figure 1. The (a) first and (b) second sea ice motion vector EOF. Colors indicate strength of each vector.

series by blending the two time series over the 7 month period January 2002–July 2002.

3. Results

[6] The interpretation of the Labrador Sea ice drift variability benefits greatly from simplifications in sea ice dynamic balance which, in general, is determined by the wind stress, the ice-ocean interfacial stress, Coriolis, and dissipative forces. The Labrador Sea ice cover is composed mostly of thin first-year ice with large fractions of new and young ice which are associated with weak internal stresses. Also the mean Labrador Sea ice drift is directed towards open ocean and not significantly hampered by land boundaries, thus the oceanic and atmospheric interfacial stresses are the primary forces. Often this type of ice motion is called ‘free drift’ where equilibrium ice motion can be solved from a simple balance between wind and ocean stress neglecting the Coriolis term (which is an order of magnitude smaller than the interfacial stresses; this balance is achieved within a few hours from initiation of a wind event):

$$\rho_a C_{ai} W^2 = \rho_w C_{wi} (u - ui)^2,$$

(ρ_a and ρ_w density of air and water; C_{ai} and C_{wi} interfacial drag coefficients; W wind speed; u and ui are ocean and ice velocities). The expression for ice velocity can be solved to be:

$$ui = u + W\sqrt{(\rho_a C_{ai}/\rho_w C_{wi})},$$

which demonstrates the division of atmospheric and oceanic forcing for the simple free drift case. Typical values of $C_{ai} = 1.5 \cdot 10^{-3}$ and $C_{wi} = 5 \cdot 10^{-3}$ give $ui = u + 2\% W$. For moderate wind speeds of 7–10 m/s, the wind driven

component of ice drift is often larger than the ocean current component (a few cm/s).

[7] With this simplification in mind, we use the EOF analysis to identify the two components of the free drift. The EOF analysis of the February–April ice drift vector fields results in two modes containing more than 90% of the total variance: 85 % and 8.3% for the first and the second modes respectively. We note that EOF analysis using a scalar ice drift gives a similar distribution of variance between the modes (88% and 8.2% respectively) (spatial patterns of scalar modes are not shown but they reflect the amplitudes of the vector modes). Also the principal components (PC’s) of the scalar drift speed are nearly identical to the principal components of the vector field. The first mode describes a unidirectional movement of the Labrador Sea/Davis Strait ice field (Figure 1a) while the second mode (Figure 1b) captures opposing ice motions between the Davis Strait region and the rest of the Labrador Sea. The first mode has the largest amplitude in the very northern part of the study region, with greatly reduced amplitude south of 62°N. The first EOF mode of the ice motion is shown to be the atmosphere-driven component.

[8] The principal components belonging to the first two modes are shown in Figures 2a–2b, where the PC’s are shown together with the averaged ice drift across the

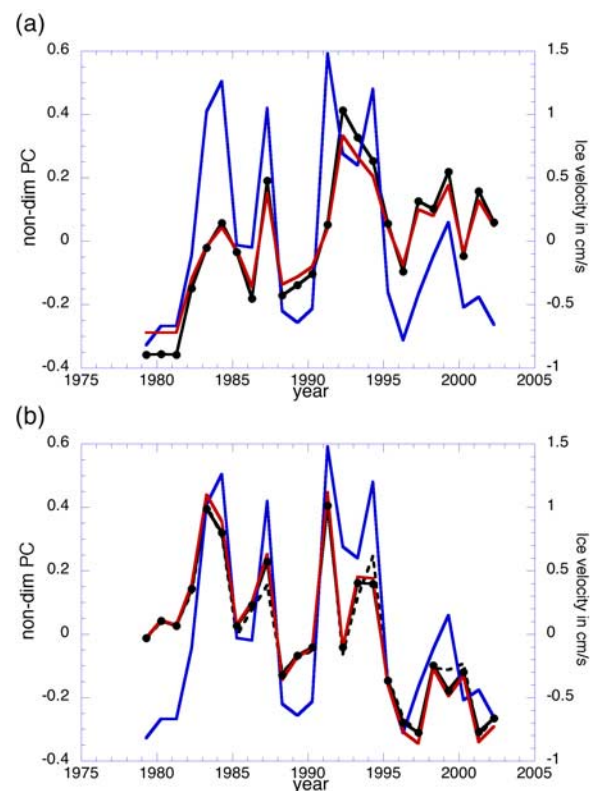


Figure 2. The time series (=principal components, PC) of the (a) first and (b) second modes of sea ice motion, denoted by black line with dots, also in (b) PC2 of the scalar ice drift field is shown (dashed black). Blue line represents the average ice drift across the Labrador shelf at 60N. Red line denotes the (a) mode 1 and (b) mode 2 contribution to the average ice velocity. PC axis on the left, the velocity axis (red and blue lines; in cm/s) on the right.

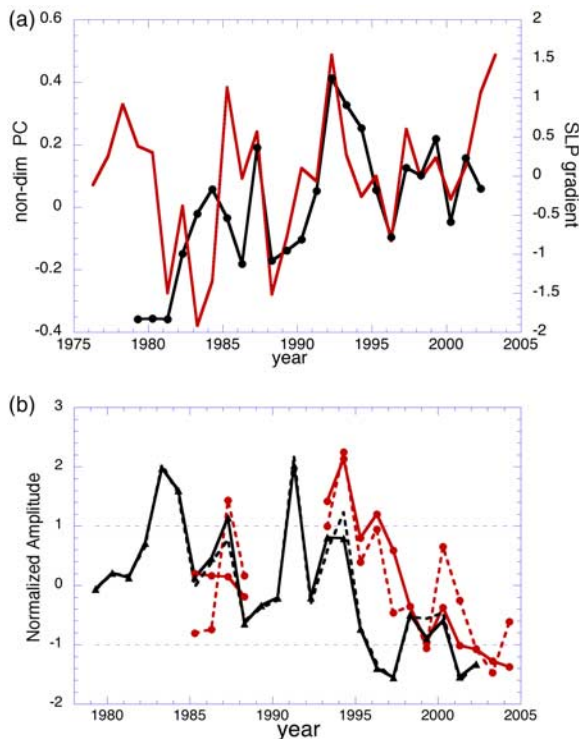


Figure 3. (a) Ice motion PC1 (black) depicted with SLP east-west gradient (red) sign reversed to have positive geostrophic wind southward. (b) Ice motion vector PC2 (black) and scalar PC2 (dashed black) depicted with the oceanic geostrophic velocity PC1 (red; the corresponding EOF1 as by Häkkinen and Rhines [2004]) and average ocean current adjacent to ice edge at 60N (dashed red), both derived from altimetry (only Feb–Apr averaged amplitudes are shown for altimetric current quantities). In (b) all time series are normalized with the corresponding standard deviation and lines at ± 1 std are marked by dashed lines.

Labrador coast, at around 60°N, to emphasize the relative contributions of the two modes in the Labrador Sea. PC1 for the scalar drift is indistinguishable from the vector field PC1, while PC2 of vector and scalar fields have slight differences. Both the first and second PCs describe a series of large fluctuations superimposed on a long-term trend of opposite signs. However, the trends are not significant because of the large fluctuations. Figures 2a–2b shows that the second mode appears to explain better the fluctuations of the ice motion at 60°N in accordance with the spatial structure of the two modes. However, both principal components contribute in varying degrees to the same multi-year variations in the ice velocity, e.g. to the maxima occurring during years 1983–1984, 1987, 1991–1994, 1998–1999.

[9] To identify the first mode as the atmosphere driven part of the sea ice drift, we compare the ice motion PC's to forcing information derived from sea level pressure (SLP) fields (NCAR SLP time series by Trenberth is used here, although the SLPs from the NCEP/NCAR Reanalysis data set give similar results). Figure 3a shows the PC1 of the sea ice motion together with the simultaneous SLP gradient between 55°W and 60°W averaged over latitude band 55°N to 65°N (the sign of SLP gradient is reversed to make the

geostrophic wind direction positive southward as in the case of ice motion). Most of the peaks in PC1 are accounted for by the SLP gradient variability, with the exception of the variations at the very beginning of the ice motion time series. After 1983 the SLP gradient is gaining an increasingly southward anomaly like PC1. A comparison with the NAO and AO indices (from NOAA/CPC), averaged from January to April, was also performed, but neither NAO nor AO provide much information on the variability of the ice motion in the study region except for the upward trend (not shown). The local SLP gradient provides a good match for the first ice motion PC, particularly after 1986 when the two curves become statistically significant at the 95% level (explaining 28% of the variance). It is also a physically attractive explanation for the first ice drift mode based on the free-drift model.

[10] It remains to be shown that the second EOF mode of the sea ice motion represents the ocean forced component. In anticipation that PC2 of the ice motion describes the influence of the ocean circulation, we can compare it to the geostrophic velocity computed from altimetry data for the North Atlantic as by Häkkinen and Rhines [2004] for the period ending July 2002. Their first EOF mode describes the variability of the currents from 30N–65N and explains the largest portion of the local variance in the subpolar gyre. The EOF analysis of the ocean velocities is updated using the Jason-1 data. The spatial part of the first mode remains the same (not shown), and the updated ocean PC1 is extended to spring 2004 indicating a continual weakening of the circulation. The ocean PC1 is shown together with the ice motion PC2 (from vector and scalar fields) and the local altimetry derived velocity off shore around 60N (Feb–Apr average). The curves are normalized with their corresponding standard deviation (std). The ice motion variations stronger than one std align with those of the ocean circulation, but the striking element of the ocean and ice curves in Figure 3b is the apparent relationship of the amplitudes of the variability throughout the last two decades: Moderate subpolar gyre strength in the mid 1980s, greater intensity in the early 1990s with a decay afterwards through 2002–2003. Figure 4 with the complete monthly ocean PC1 time series shows that the late 1970s also have a

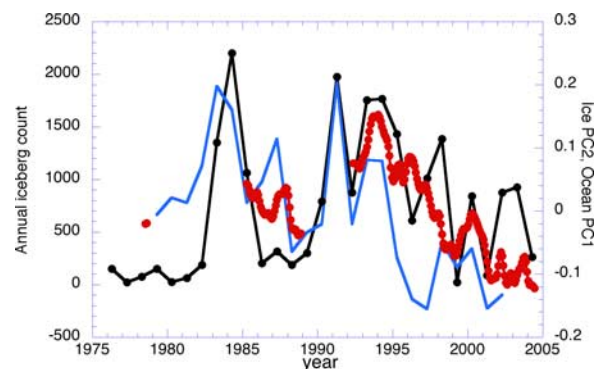


Figure 4. The annual iceberg count crossing 48°N (black; axis on the left) is shown with the ice motion PC2 (blue) and with the ocean velocity PC1 (red; all months are shown). The ice motion PC2 is scaled by 0.5 to match the scale of the ocean PC1 on the right.

moderate gyre strength inline with the ice drift PC2 variability. The ocean vector mode and the local altimetry-derived ocean current at 60N explain 36% and 50% of the variance respectively in the ice drift PC2 after 1992 (the latter relationship is statistically significant at the 95% level; the altimetry data from earlier years are not as accurate as TOPEX/Poseidon and Jason-1 altimeters, thus we give correlations only for the latter period). The coincident, larger than one std fluctuations of the ice motion and altimetric velocity suggest that the gyre-scale changes depicted by the altimetric mode extend their influence to the near coastal circulation also (where altimeter data is not available due to ice cover). From Figure 3b it appears that significant changes in the subpolar gyre such as in the beginning of the 1980s and in 1991 were missed because of gaps in the altimetry data record. Most importantly, the ice motion PC2 and the original ice drift data from Labrador Sea provide an independent, long, and continuous time series supporting the ocean circulation changes inferred from altimetry particularly for the 1990s and the early 2000s.

[11] Another source of information on the ocean circulation changes is provided by the tracking of icebergs, although there is some uncertainty as to how much the recorded number of icebergs crossing latitude 48°N depends on the count of released icebergs in western Greenland. The iceberg count crossing 48°N shown with the ice motion PC2 and the ocean velocity PC1 in Figure 4 suggests that the three largest peaks in iceberg count are present in the ice motion PC2 and ocean PC1, except the moderate (4th largest) 1998 peak. Thus, despite possible uncertainties in released icebergs in the source region, the drift current intensity is largely responsible for the major iceberg crossing 48°N events during the thirty-year period.

4. Discussion

[12] We have investigated Labrador Sea ice motion for the last 24 years derived from satellite data sets by Fowler [2003]. The accuracy of the Labrador ice drift from satellite data is difficult to assess due to sparse in situ observations. However, we can capture the largest fluctuations by applying EOF analysis which selects dominant features, temporally and spatially, and thereby reduce the impact of inherent uncertainties in the ice motion analysis. Labrador Sea ice motion fields are shown to separate into atmospheric and oceanic driven parts using EOF analysis. Our analysis suggests that the wind driven ice drift in the Labrador Sea explains over 85% of the ice motion variance whereas about 8% can be explained by the ocean driven drift. Together

they explain over 90% of the variance which confirms that the free-drift approximation provides a good estimate of sea ice motion in this region. The association of the first mode to wind forcing is based on an east-west SLP gradient over the analysis region. However, no straightforward connection to NAO or AO variability is detected. The ocean driven component of the sea ice drift is determined from comparison of the ice drift PC2 with the first altimetric velocity mode. The two time series contain similar broad features through almost three decades confirming the amplitude variations seen in the altimetric velocity record of Häkkinen and Rhines [2004]. Thus, the ice motion data provide an independent data source to support the ocean circulation changes seen from altimetry in the northern North Atlantic Ocean where long term (over decades) current meter data is lacking. Another independent data source is the iceberg count crossing 48°N latitude. Since 90% of iceberg mass is below sea level, it is fair to expect that the ocean currents would dominate the iceberg drift. This relationship can be hampered by the variations in the number of icebergs released from West Greenland. Despite this potential limitation, the iceberg count variability is similar to that observed in the oceanic component of the ice drift and to that of the altimetric velocity mode.

[13] **Acknowledgments.** This work has been supported by the NASA Headquarters Physical Oceanography and Polar Programs. Authors thank Prof. Peter Rhines for useful comments to improve the manuscript. Also the authors want to thank Ms Denise Worthen for assistance with graphics.

References

- Cavalieri, D. J., C. L. Parkinson, and K. Y. Vinnikov (2003), 30-year satellite record reveals contrasting Arctic and Antarctic decadal sea ice variability, *Geophys. Res. Lett.*, *30*(18), 1970, doi:10.1029/2003GL018031.
- Fowler, C. (2003), *Polar Pathfinder Daily 25 km EASE-Grid Sea Ice Motion Vectors*, Natl. Snow and Ice Data Cent., Boulder, Colo. (Available at <http://nsidc.org/data/nsidc-0116.html>.)
- Häkkinen, S., and P. B. Rhines (2004), Decline of subpolar North Atlantic gyre circulation during the 1990s, *Science*, *304*, 555–559.
- Han, G., and C. L. Tang (2001), Interannual variations of volume transport in the western Labrador Sea based on TOPEX/Poseidon and WOCE data, *J. Phys. Oceanogr.*, *31*, 199–211.
- Parkinson, C. L., and D. J. Cavalieri (2002), A 21-year record of Arctic sea ice extents and their regional, seasonal, and monthly variability and trends, *Ann. Glaciol.*, *34*, 441–446.
- Yu, Y., G. A. Maykut, and D. A. Rothrock (2004), Changes in the thickness distribution of Arctic sea ice between 1958–1970 and 1993–1997, *J. Geophys. Res.*, *109*, C08004, doi:10.1029/2003JC001982.

D. J. Cavalieri and S. Häkkinen, NASA Goddard Space Flight Center, Greenbelt, MD 20771, USA. (sipa.hakkinen@nasa.gov)